

Article

Preparation and Properties of Phosphoric Acid-Based Porous Geopolymer with High Magnesium Nickel Slag and Fly Ash

Xingchun Yang ¹, Yuan Wu ¹, Zhigao Sun ¹, Yufeng Li ¹, Dongsheng Jia ¹, Dongliang Zhang ¹, Dehua Xiong ² and Mitang Wang ^{1,*}

¹ School of Materials and Chemistry, University of Shanghai for Science and Technology, Shanghai 200093, China; 202342982@st.usst.edu.cn (X.Y.)

² State Key Laboratory of Silicate Materials for Architecture, Wuhan University of Technology, Wuhan 430070, China

* Correspondence: btwmt@126.com

Abstract: Phosphoric acid-based porous geopolymers were prepared by two different foaming agents (H₂O₂ and Al powder) with phosphoric acid as the activator. High-magnesium nickel slag (HMNS) and fly ash (FA) were the precursor combination. The effects of foaming agent types and contents on the properties of HMNS-FA-phosphate-based porous geopolymers were investigated in terms of dry density, pore structure, compressive strength, thermal conductivity, and water absorption. The phase was analyzed by x-ray diffraction (XRD) and Fourier transform infrared spectroscopy (FT-IR). It was found that both foaming agents could successfully prepare porous geopolymers, and the compressive strength and dry density of porous geopolymers gradually decreased and the low-thermal conductivity and water absorption gradually increased with the increase in foaming agent content. The foaming agents formed porous structures inside porous geopolymers but did not affect the phases of geopolymerization reactions. This study demonstrates that both foaming agents can be used to prepare HMNS-FA-phosphate-based porous geopolymers for the application of phosphate-activated geopolymers in the direction of refractory materials.

Keywords: porous geopolymer; HMNS; phosphoric acid; geopolymerization

Citation: Yang, X.; Wu, Y.; Sun, Z.; Li, Y.; Jia, D.; Zhang, D.; Xiong, D.; Wang, M. Preparation and Properties of Phosphoric Acid-Based Porous Geopolymer with High Magnesium Nickel Slag and Fly Ash. *Minerals* **2023**, *13*, 564. <https://doi.org/10.3390/min13040564>

Academic Editors: M Akbar Rhamdhani, Wentao Hu, Hong Peng

Received: 13 March 2023

Revised: 31 March 2023

Accepted: 15 April 2023

Published: 17 April 2023



Copyright: © 2023 by the authors. Licensee MDPI, Basel, Switzerland. This article is an open access article distributed under the terms and conditions of the Creative Commons Attribution (CC BY) license (<https://creativecommons.org/licenses/by/4.0/>).

1. Introduction

Porous geopolymers are a new type of polymer material, mainly composed of aluminum and silicon, and made of clay, industrial waste, or slag as raw materials. It was developed by French chemist J. Davidovits [1] in the 1970s, mainly through the polymerization of oxygen-containing tetrahedra using appropriate processes at a lower temperature (50–180 °C) through chemical reactions with great compressive strength. This type of polymer is a new material with a wide range of prospects. The total amount of CO₂ emitted by traditional silicate cement is about 0.82 t for every 1 t of clinker produced [2]. A geopolymer as a new gel material to partially replace cement has important research implications for a reduction in CO₂ emissions [3–6].

Porous geopolymer research has grown exponentially over the last decade (2010–2020). From 2010 to 2014, it focused on characterizing porous geopolymers from both chemical and physical aspects [7–11]. The amorphous and crystalline phases of the reaction products were characterized by different methods, and the products were chemically characterized. Physical characterizations were commonly researched in the course of this stage [3]. Research during this period extensively evaluated these properties along with the constituent materials. A trend started during this period, between 2014 and 2017, where porous geopolymers made from newer raw materials were used [12–16]. Regarding properties, fire resistance started to receive primary attention [16–23]. The extensive global interest in porous geopolymers during 2017–2022 led to an evident increase in the

number of research papers. In this period, new foaming technologies [24–26] were extensively investigated. Foam stabilizers (e.g., SDS) added to geopolymer-based blends during chemical foaming [27–29] and thickeners added to preformed foams during mechanical foaming enhanced the stability of pores [30].

Porous geopolymer properties have been discussed by many scholars [31,32]. Gu et al. [33] measured and analyzed the influence of foam content on the dry density, compressive strength, and thermal conductivity of porous geopolymers.

With the increasing global production of stainless steel in recent years, large amounts of high-magnesium nickel slag (HMNS) have been deposited in landfills, causing soil and groundwater pollution. Some studies have shown that HMNS has good thermal stability and the potential to prepare high-temperature resistant materials [34,35], indicating that porous materials made from HMNS can capitalize on its unique characteristics.

However, there have been few studies on porous geopolymer made from HMNS due to its low reactivity with activators at room temperature. Moreover, most studies on porous geopolymers have been focused on alkali solutions [36–41]. These two reasons have contributed to the scarcity of research on HMNS porous geopolymer and phosphoric acid excitation. FA raises the alkalinity of the geopolymerization reaction as part of the precursor and not only causes a large waste of land resources but also causes a variety of problems, such as water and soil pollution, land pH imbalance, and affects the living environment of plants and animals [42].

This study is expected to encourage further research on HMNS and reduce pollution caused by HMNS and FA. Porous geopolymers were prepared by utilizing geopolymer technology with HMNS and fly ash as raw materials, H_2O_2 and Al powder as foaming agents, sodium dodecyl sulfate (SDS) as a foam stabilizer, and phosphoric acid as the activator. The major chemical components of raw materials were SiO_2 and MgO . The content of foaming agents was regulated to prepare the porous geopolymer, and the effect of blowing agents on porous geopolymers was examined. The physical properties of porous geopolymers were discussed, and the reaction mechanism of the porous geopolymer was summarized based on the microscopic analysis results.

2. Materials and Methods

2.1. Raw Materials

The HMNS and FA, obtained from the Baotou factory (Baotou, China), have a high content of silicon and magnesium. HMNS was grounded and screened (100 mesh). The main chemical components of them are shown in Table 1. Figure 1 is the SEM image of HMNS and FA, and Figure 2 is the XRD pattern of HMNS and FA. The major crystal phases in high-magnesium nickel slag are forsterite, ferrosilite, magnesium silicate, and quartz, while the major crystal phases in FA are quartz and mullite, with the potential to prepare cementitious materials. Table 1 shows the major chemical constituents of FA are SiO_2 , Al_2O_3 , and CaO , while the major chemical constituents of HMNS are SiO_2 , MgO , Fe_2O_3 , and Al_2O_3 .

The phosphate activator is 85% pure and comes from Shanghai, China. The purity of H_2O_2 (from Shanghai, China) is 30%. SDS and Al powder (99% by mass) are both analytical reagents. All of the industrialized products were purchased from Sinopharm Chemical Reagent Co., Ltd. (Shanghai, China). Deionized water was used throughout the experiment. Allow the mixture to cool for 24 hours at room temperature before using. In this study, H_2O_2 and Al powder were selected as foaming agents, and different contents of H_2O_2 and Al powder were designed to prepare porous geopolymers. The ratio of HMNS to FA was 7:3, the content of SDS was 0.1%, and the content of phosphoric acid was 20%. The experimental design is shown in Table 2.

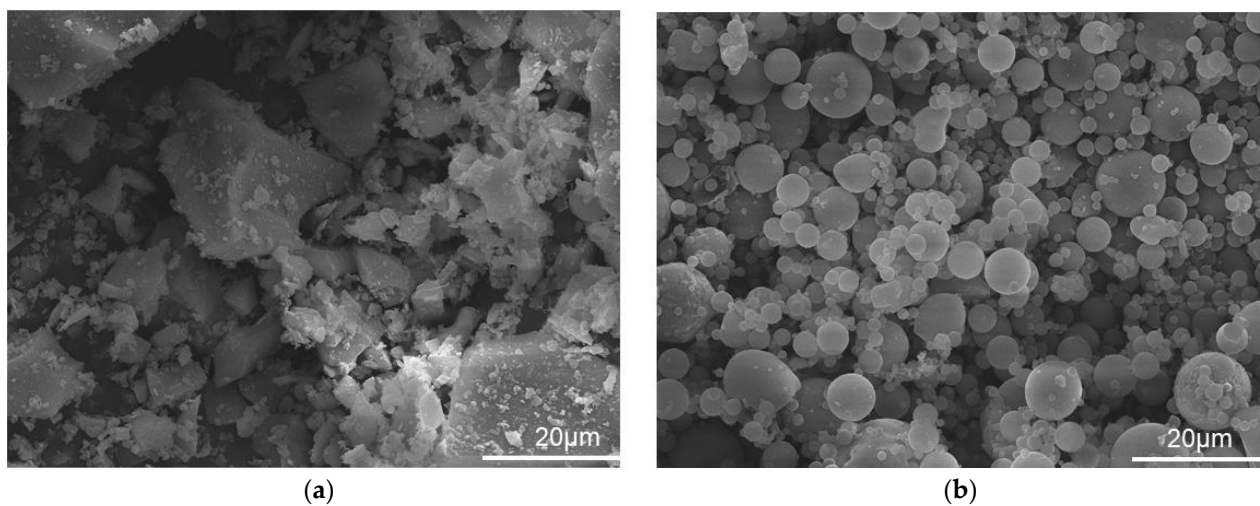


Figure 1. SEM images of (a) HMNS and (b) FA.

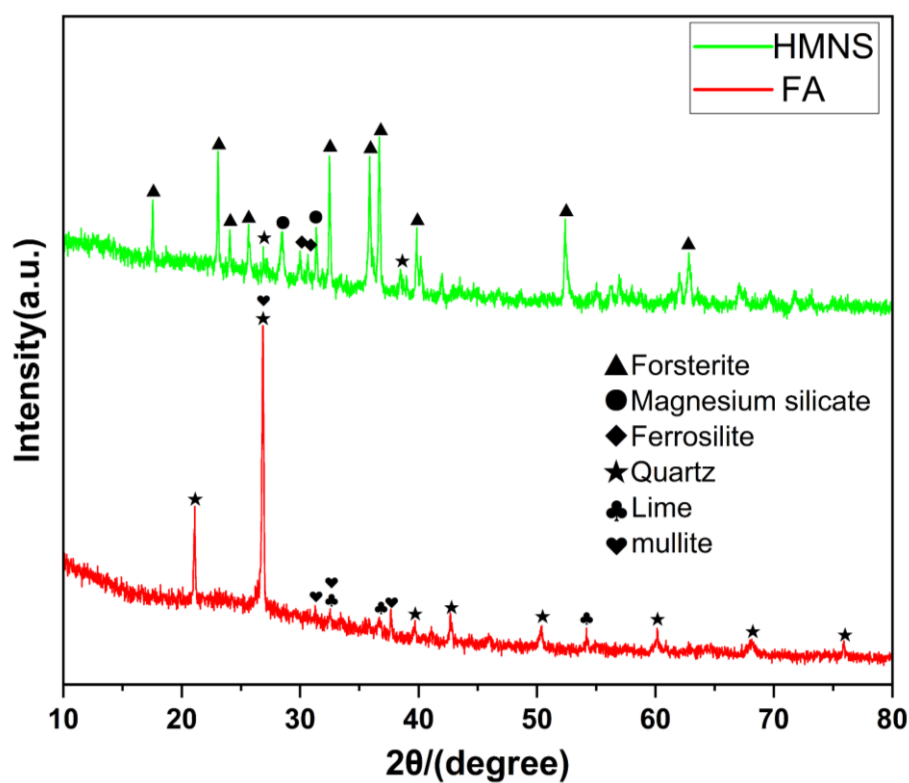


Figure 2. XRD patterns of HMNS and FA.

Table 1. Chemical composition of HMNS and FA.

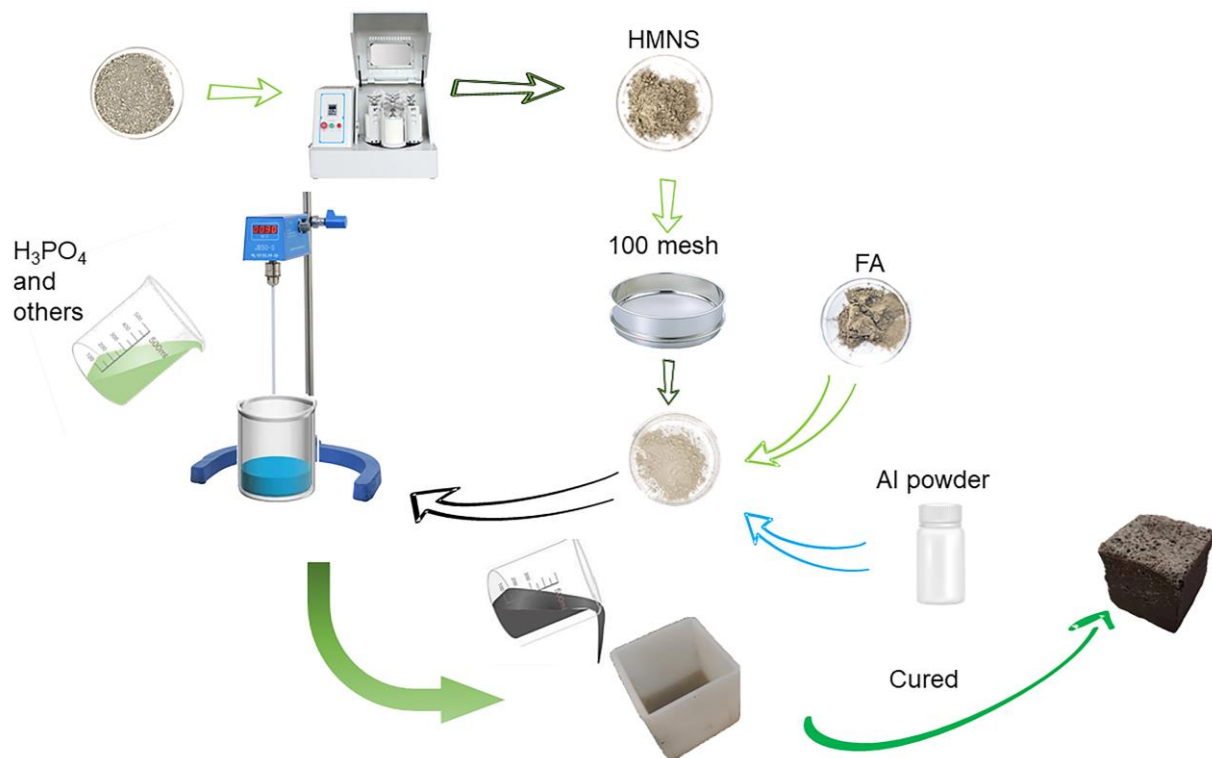
Oxide	SiO ₂	MgO	Fe ₂ O ₃	Al ₂ O ₃	CaO	MnO	K ₂ O	Na ₂ O	Cr ₂ O ₃
HMNS	46.66	26.53	14.01	8.44	0.92	0.69	0.13	n.d.	1.93
FA	53.33	1.97	8.43	19.64	11.72	0.09	1.17	0.829	-

Table 2. Experimental design.

Sample	H ₂ O ₂					Al				
	1	2	3	4	5	1	2	3	4	5
HMNS/FA					7/3					
SDS					0.1%					
H ₃ PO ₄					20%					
Content(H ₂ O ₂ /Al)	0	0.2	0.4	0.6	0.8	0	0.02	0.04	0.06	0.08

2.2. Sample Preparation

As shown in Figure 3, the HMNS used in this work were air-cooled after being coarsely ground to particulate matter, and then they were passed through a 200-mesh (75 μ m) sieve. In this study, FA was directly used without processing. As shown in Table 2, Al powder and H₂O₂ were added in different mass fractions.

**Figure 3.** Preparation process of porous geopolymers.

2.2.1. Preparation Process When H₂O₂ Is Used as a Blowing Agent

The acid activator was prepared according to the planned procedure and allowed to stand for one hour before use. HMNS and FA were weighed and stirred in a plastic beaker using a glass rod. In deionized water, H₂O₂ and SDS were added and mixed to form a slurry. Subsequently, the mixed solids were slowly added into the slurry, and then the acid activator was slowly poured in as well. The resulting foam slurry was mixed thoroughly using an electric stirrer. The slurry was then rapidly injected into a 20 mm \times 20 mm \times 20 mm mold.

2.2.2. Preparation Process When Al Powder Is Used as a Blowing Agent

The acid activator was first prepared according to the planned procedure and left to stand for a duration of 1 hour before use. Subsequently, the required amounts of HMNS, FA, and Al powder were weighed out and stirred together using a glass rod in a plastic beaker.

Next, SDS was added to deionized water to create a solution, into which the mixed solids were poured to form a homogenous slurry. The acid activator was then added to the slurry in a slow, gradual manner while continuously mixing the contents using an electric stirrer. The aim of this step was to achieve a uniformly dispersed foam slurry.

Finally, the resulting slurry was swiftly and accurately injected into a mold with dimensions of 20 mm × 20 mm × 20 mm.

The porous geopolymer was demolded for about one day (in an oven at 40 °C) after casting. The tested specimens were cured for 7 days. Sample fragments collected from compression tests were used for XRD and FTIR.

2.3. Analytical Method

The specimens for the dry density test are dried in a drying oven at 60 °C. Dry density is calculated according to Equation (1):

$$\rho_0 = \frac{m_0}{V} \quad (1)$$

ρ_0 = dry density in kilograms per cubic meter (kg/m³); m_0 = the drying mass of the specimen in kilograms (kg); V = the volume of the specimen in cubic millimeters (m³). The size of the specimen of porous geopolymer used for the strength test was 20 mm × 20 mm × 20 mm. The average value of 3 samples was taken for the final property result. The compressive strength test method was carried out according to ASTM C109/C109M-2013. A DYE-300 microcomputer servo press was used to determine the compressive strength of the porous geopolymer samples. A LFA-467 thermal conductivity meter was used to test the thermal conductivity of the porous geopolymers. DSC was tested by Mettler Toledo TGA/DSC 3+. The specimens were made into thin sheets and tested in a 25 °C environment.

First, the specimens for the dry density test were weighed after drying in a drying oven at 60 °C. Then, the specimens were weighed after being placed in a constant-temperature water bath for 24 hours. Water absorption is calculated by Equation (2):

$$W_R = \frac{m_g - m_o}{m_o} \quad (2)$$

W_R = water absorption (%), calculated accurately to 0.1; m_o = mass of specimen after drying, in kilograms (kg); m_g = mass of specimen after water absorption, in kilograms (kg). The scanning range of the X-ray diffractometer (XRD) with CuK α radiation is 10°~80°. The FT-IR spectra were recorded over a range of 4000 cm⁻¹ to 400 cm⁻¹.

3. Results and Discussion

3.1. Physical Properties

3.1.1. Dry Density

The effect of blowing agent content and type on the dry density of porous geopolymers was investigated. As can be seen from Figure 4, the dry density of porous geopolymers was 822 kg/m³ at the highest and 664 kg/m³ at the lowest when H₂O₂ was used as the foaming agent. When Al powder was used as the foaming agent, the dry densities of the geopolymers were 1130 kg/m³ and 772 kg/m³, respectively. It is easy to see that the Al powder only needs to be added in lesser amounts than H₂O₂ to achieve a similar dry density.

When the two blowing agent content elevation rates are the same, the decreasing trend of the specimens foamed with Al powder is significantly smoother. This may be because the liquid form of the foaming agent can produce foam earlier and faster compared to the solid form. When HMNS, FA, and phosphoric acid are fully mixed to form a slurry, the addition of H₂O₂ generates oxygen more quickly and is more likely to produce more foam during curing. That is also the reason why the dry density of porous geopolymer prepared by H₂O₂ is lower.

The dry density of porous geopolymers showed a constant decrease with increasing blowing agent content, whether H_2O_2 or Al powder was used as the blowing agent. Due to the increasing amount of blowing agent, more foam is continuously generated during the curing process of the geopolymers. These foams generate larger, more numerous pores inside the geopolymer as the blowing agent content increases and the reaction products grow around the pores formed by the blowing agent at the beginning of curing. This eventually forms a porous geopolymer containing many pores. The most direct macroscopic manifestation of this phenomenon is the decrease in dry density. However, the dry density does not always decrease as the blowing agent content increases because porous geopolymers are difficult to prepare successfully with the addition of excess blowing agent.

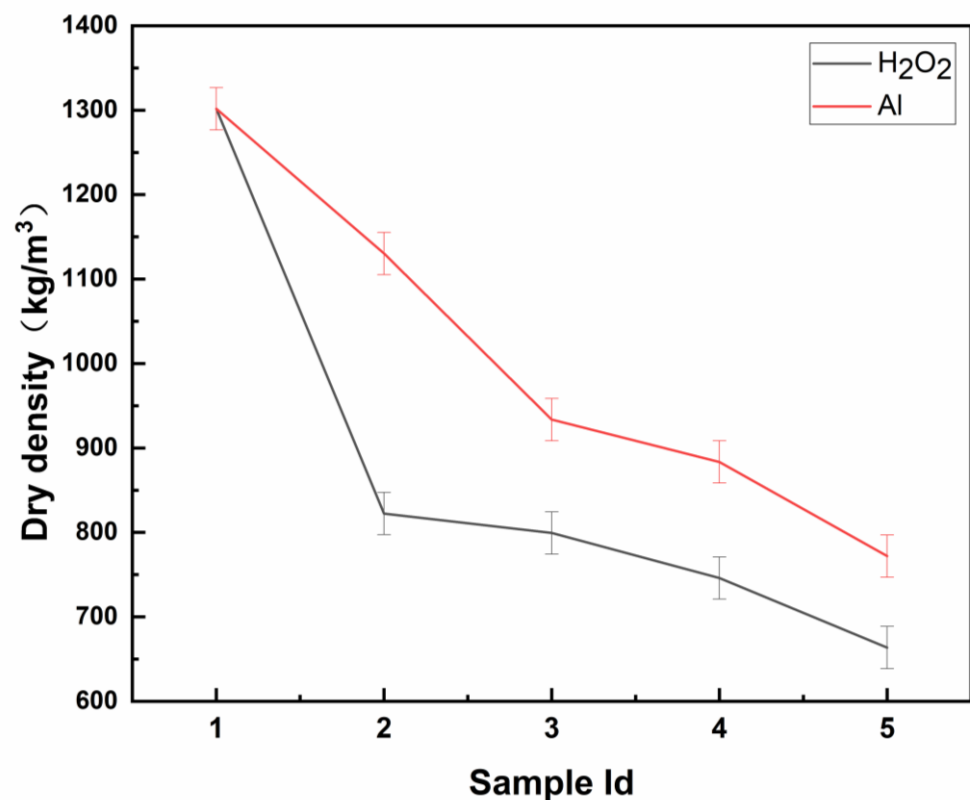


Figure 4. Influence of type and content of the foaming agent on the dry density of porous geopolymers.

3.1.2. Pore Structure

The pore structure was found to change as the type and content of the blowing agent changed. More pores are produced when the content of the blowing agent increases, regardless of the type of blowing agent, as seen in Figure 5. The bubbles generated by the chemical reaction are rapidly immobilized in the geopolymer due to the rapid acid-base neutralization reaction. The number of pore structures increases due to more bubbles being trapped.

Pores with a diameter of more than 0.5 mm are found in porous geopolymers due to the fusion of small bubbles with each other when there is an increase in the foaming agent. The number of open pores also increased due to the increase in pore structure, which resulted in smaller spacing between pores. The change in pore structure leads to a change in the physical properties of the porous geopolymers, such as the dry density discussed previously. This trend of change is corroborated with the trend of change in dry density. The higher number of pores and smaller pore spacing resulted in a lower dry density of the specimens prepared by H_2O_2 foaming.

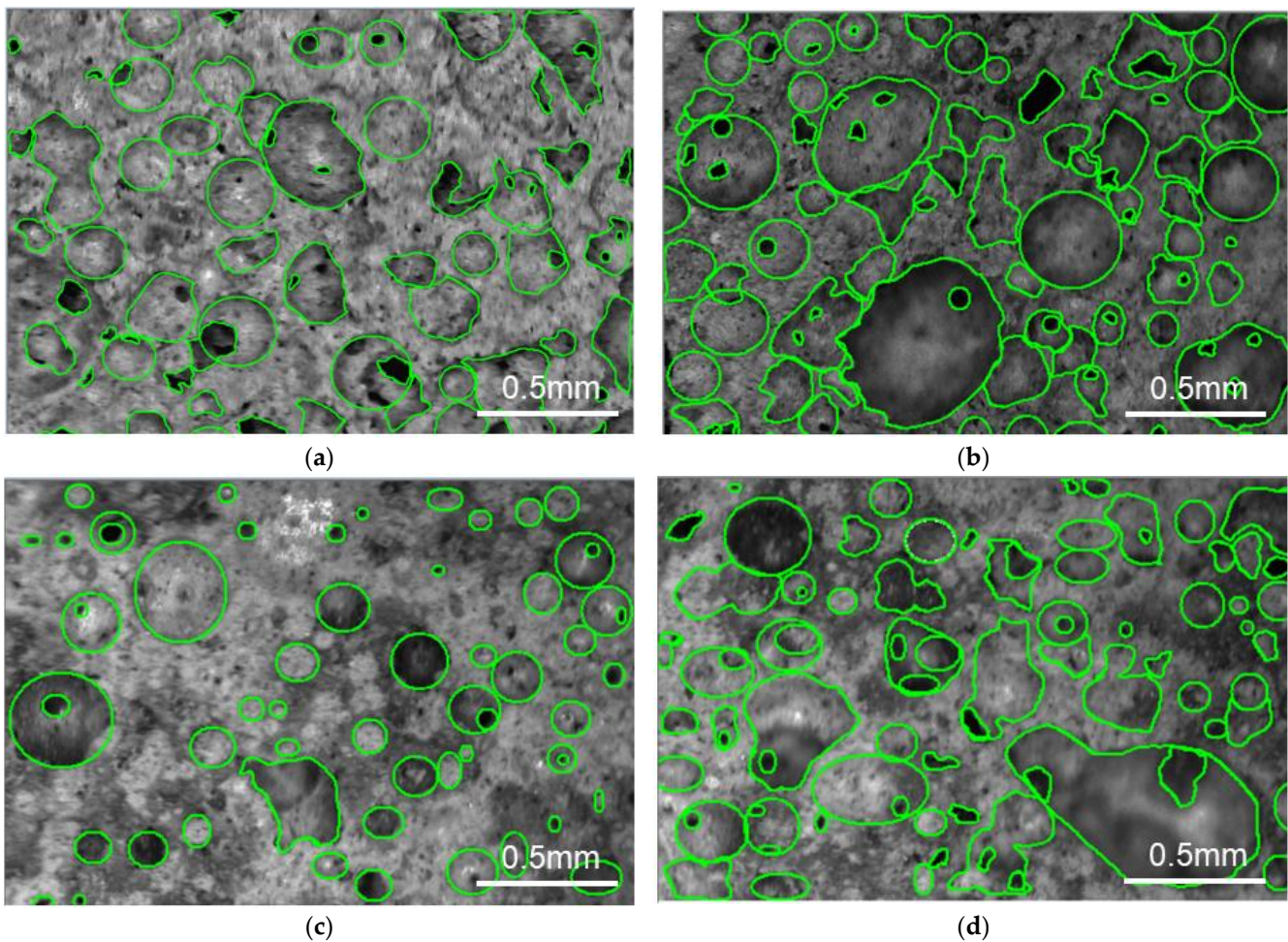


Figure 5. Photographs of HMNS-FA-phosphate-based porous geopolymers. (a) 0.2% H₂O₂, (b) 0.8% H₂O₂, (c) 0.02% Al, and (d) 0.08% Al.

3.1.3. Compressive Strength

The compressive strength of the specimens was tested. This was carried out to investigate the effect of the type and content of the blowing agent on the porous geopolymer. As can be seen from Figure 6a, the compressive strength of the porous geopolymer prepared by two blowing agents decreased with the increase in the blowing agent content after 3 days of curing. After 3 days of curing, the compressive strength of the specimens prepared with H₂O₂ as the blowing agent was 2 MPa at the highest and 0.4 MPa at the lowest. The compressive strength of the specimens prepared with Al powder as the blowing agent was 1.2 MPa at the highest and 0.8 MPa at the lowest.

As can be seen from Figure 6b, the compressive strength of HMNS-FA-phosphate-based porous geopolymer prepared by both blowing agents gradually decreased with the increase in the blowing agent content after 7 days of curing. The compressive strength of the specimens prepared with H₂O₂ was 2.8 MPa at the highest and 0.8 MPa at the lowest. The compressive strength of the specimens prepared with Al powder was 2 MPa at the highest and 1.2 MPa at the lowest.

From Figure 6a,b, it can be seen that when both foaming agents were added in the third gradient, the compressive strength of the specimens prepared with H₂O₂ was higher than that of the specimens prepared with Al powder after 3 days of curing. However, after 7 days of curing, both of them had the same compressive strength. When the content of the blowing agent added was in the fourth gradient, the compressive strength of the specimens prepared by Al powder was the same as that of the specimens prepared by H₂O₂ after 3 days of curing. However, after 7 days of curing, the compressive strength of the

specimens prepared by Al powder was higher than the specimens prepared by H₂O₂. This phenomenon occurs because the Al powder produces a denser porous structure with smaller pores. The compressive strength of porous geopolymers with small pores will have better rising potential.

We can learn from Figure 7 that the compressive strength of the porous geopolymers prepared by both foaming agents increased with an increase in curing time. The best specimen prepared with H₂O₂ had a compressive strength of up to 2.8 MPa, and the best specimen prepared with Al powder had a compressive strength of up to 2 MPa. During the maintenance period, the incompletely reacted phosphoric acid continues to participate in the geopolymerization reaction. Therefore, the strength of the porous geopolymer increases. A phenomenon that can be concluded from Figure 7 is that a geopolymer without an added foaming agent has a higher compressive strength. This is because the geopolymer without an added blowing agent has no pore structure. This indicates that it contains more unreacted than reacted material. Meanwhile, the unreacted material continues the geopolymerization process. At the same time, the porous structure of the geopolymer has more contact area with air; the phosphoric acid is dissolved by the water in the air, and the reduction in phosphoric acid reduces the degree of late reaction. The reduction in the generated product reduces the compressive strength of the specimen.

From Figure 8, we can see that compressive strength shows a decreasing trend with the increase in blowing agent content. The compressive strength of the porous geopolymers prepared by the two foaming agents is similar when the dry densities are the same. It suggests that the type of blowing agent may not have a negative impact on the strength of porous geopolymers.

With the geopolymerization reaction fully carried out, the compressive strength of the specimens prepared with Al powder was better enhanced after seven days of maintenance. H₂O₂ can be chosen for the preparation of porous materials when the need for compressive strength is greater than the requirement for dry density. Al powder can be chosen for the preparation of porous materials when a better dry density is desired.

The strength of porous geopolymers is influenced by various factors. The acid-activated geopolymerization process is based on the acid-base neutralization reaction [43], and the acid-base neutralization reaction gives a high early strength to the specimen. The porous structure retards the geopolymerization reaction at an early stage, resulting in a decrease in compressive strength. However, as the curing time increases, more gel phases are generated, which increases the strength of the porous geopolymer.

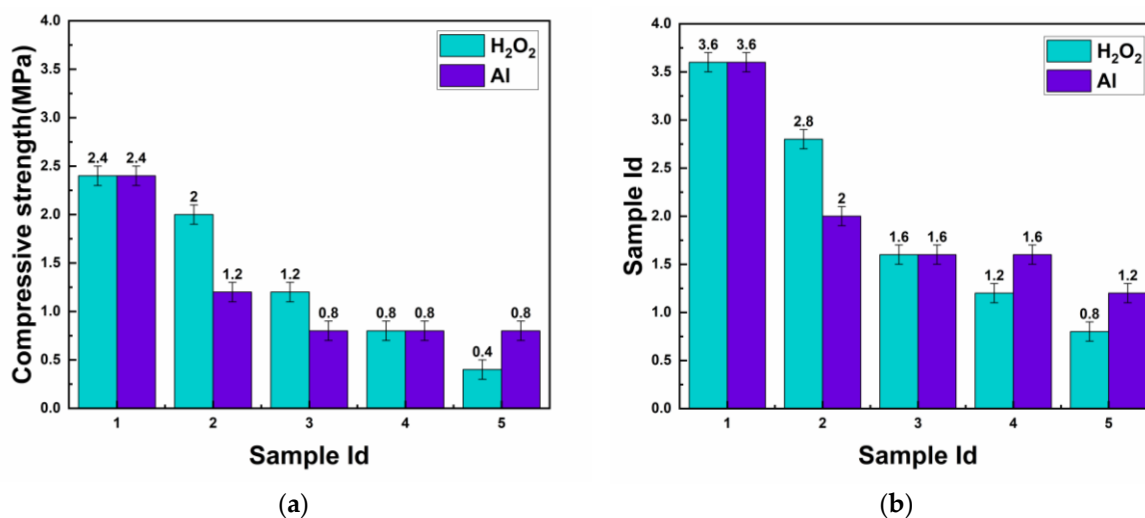


Figure 6. Effect of the type and content of the foaming agent on the compressive strength of porous geopolymers. (a) 3 days and (b) 7 days.

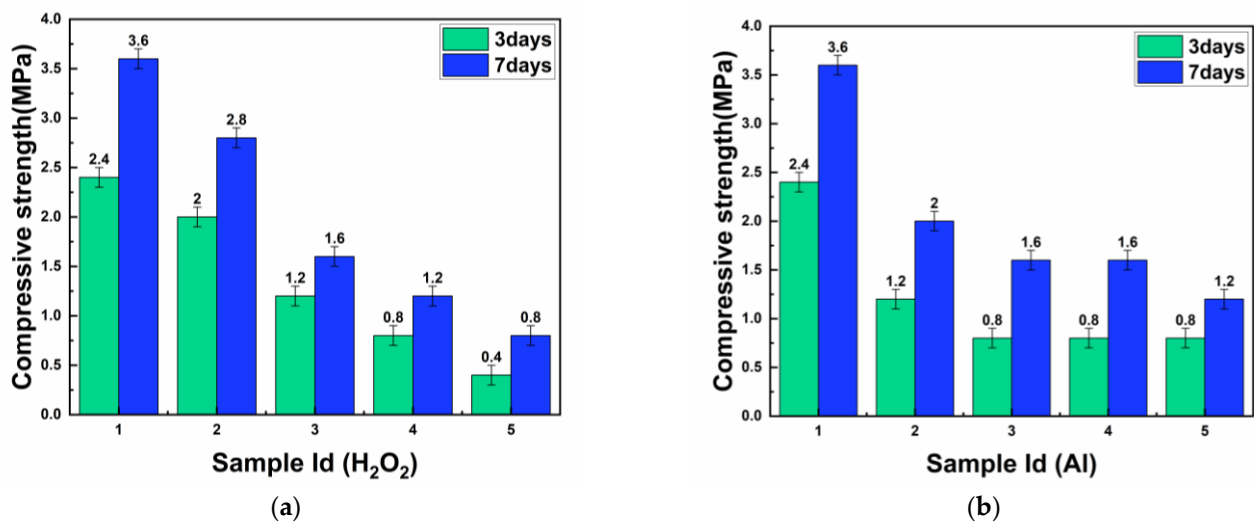


Figure 7. Effect of curing time on the compressive strength of porous geopolymers. (a) H₂O₂ foaming and (b) Al foaming.

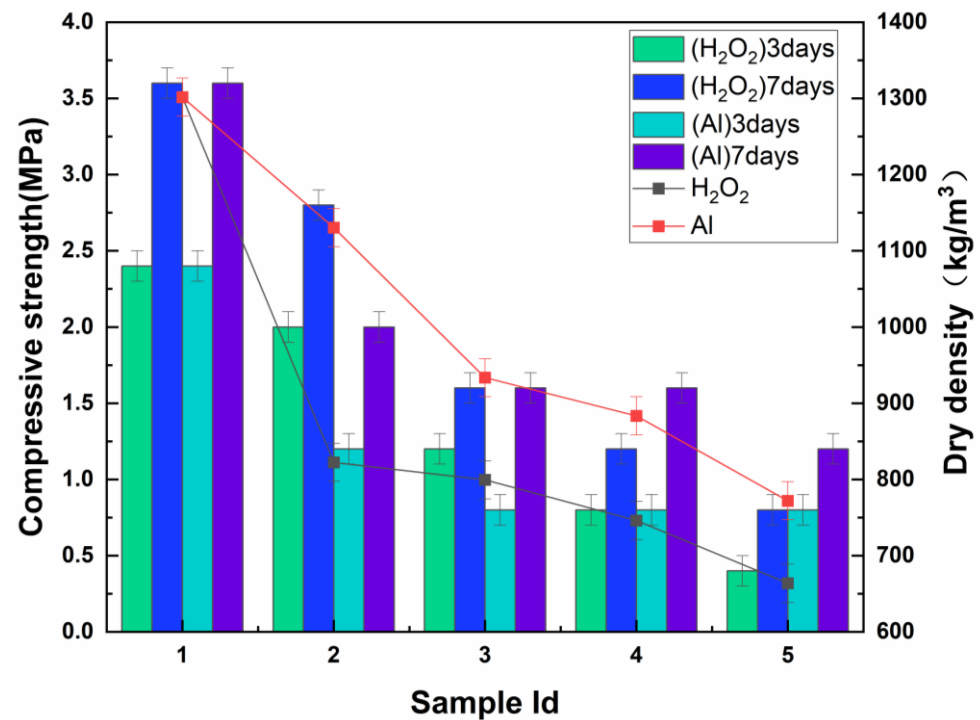


Figure 8. Relationship between the compressive strength and dry density of HMNS-FA-phosphate-based porous geopolymers.

3.1.4. Thermal Conductivity DSC Analysis

Thermal conductivity was tested to investigate the effect of blowing agents on porous geopolymers. As shown in Figure 9, the thermal conductivity of HMNS-FA-phosphoric acid-based porous geopolymers keeps decreasing. When no foaming agent was added, the thermal conductivity was 0.87 W/Mk. After adding H₂O₂ and Al powder, the thermal conductivity of the phosphate porous geopolymers reached a minimum of 0.25 W/Mk and 0.19 W/Mk, respectively.

Additionally, it is easy to see from the graph that HMNS-FA-phosphoric acid geopolymers become a porous material with a low dry density and good low-thermal conductivity even with the addition of a minimum amount of H₂O₂ or Al powder. This gives HMNS-FA-phosphate geopolymers great potential in the field of insulation and refractory

materials, such as insulation and fireproofing materials for buildings. The thermal conductivity of geopolymers can be significantly reduced by the addition of either blowing agent, and an increase in the content of both blowing agents results in better low-thermal conductivity. This is because the foam is rapidly distributed into the geopolymer with the rapid occurrence of the pre-depolymerization reaction and sufficient mixing when the blowing agent is added. As the blowing agent content increases, more foam is produced, which results in more pores in the geopolymer, and these pores bring about an improvement in low-thermal conductivity.

From Figure 9, it can be seen that when the dry density of porous geopolymers prepared by two different blowing agents is similar, the thermal conductivity of both is also similar. This indicates that the type of blowing agent does not produce a phase that affects the low thermal conductivity of the geopolymer.

Figure 10 illustrates the differential scanning calorimetry (DSC) curves obtained from specimens that were prepared with and without foaming agents. Notably, an exothermic peak was observed at approximately 683 °C, which is attributed to the decomposition and rearrangement of magnesium pyrophosphate ($Mg_2P_2O_7$)_n into magnesium pyrophosphate units ($Mg_2P_2O_7$) [44]. Except for the absorption peaks of free and bound water at around 129 °C, no endothermic peaks were detected prior to 800 °C. The findings illustrate the exceptional thermal stability of the geopolymer with a porous structure, which maintains its structural integrity even at elevated temperatures of up to 800 °C.

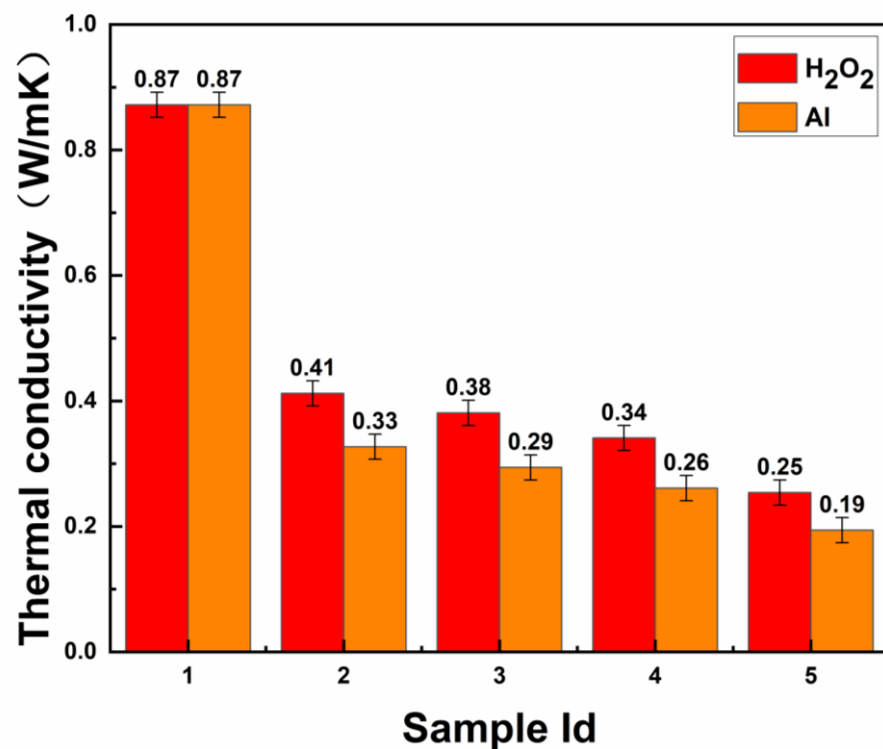


Figure 9. Thermal conductivity of HMNS-FA-phosphate-based porous geopolymers.

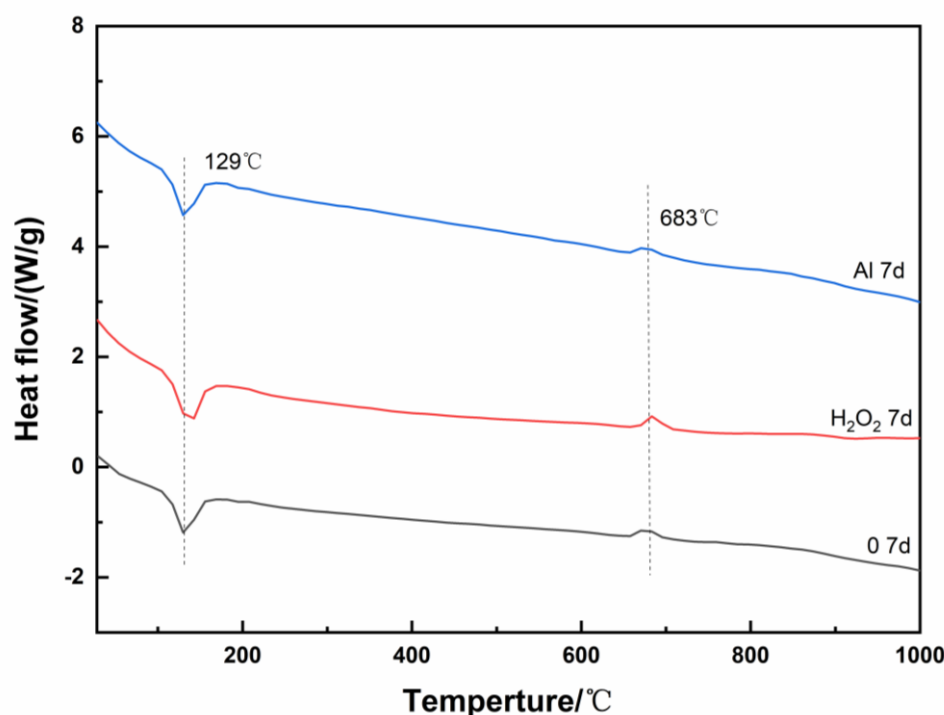


Figure 10. DSC of HMNS-FA-phosphate-based porous geopolymers.

3.1.5. Water Absorption Performance

The water absorption properties of porous geopolymers were tested. As shown in Figure 11, the water absorption of porous geopolymers showed a rising trend. When the amount of Al powder added is 0.02%, the water absorption rate is 30.6%; the water absorption rate is nearly double that of the specimen without a foaming agent. When the amount of H₂O₂ added is 0.2%, the water absorption rate increases to 50%, which is more than three times that of the specimen without a foaming agent. This also indicates that a porous structure can be formed inside the geopolymer by adding a small amount of foaming agent. This structure causes the dry density of the geopolymer to decrease. As shown in Figure 5, the porous geopolymer has a pore structure inside. The water absorption of the specimen increases because the porous structure preserves a large amount of water.

The water absorption of the specimen with the addition of Al powder was higher when the porous geopolymer prepared by the two blowing agents had the same dry density. This is because the porous geopolymer has fewer open pores when Al powder is used as the blowing agent. Porous geopolymers can be used as water storage materials, depending on the pore characteristics of the specimens prepared with the two blowing agents.

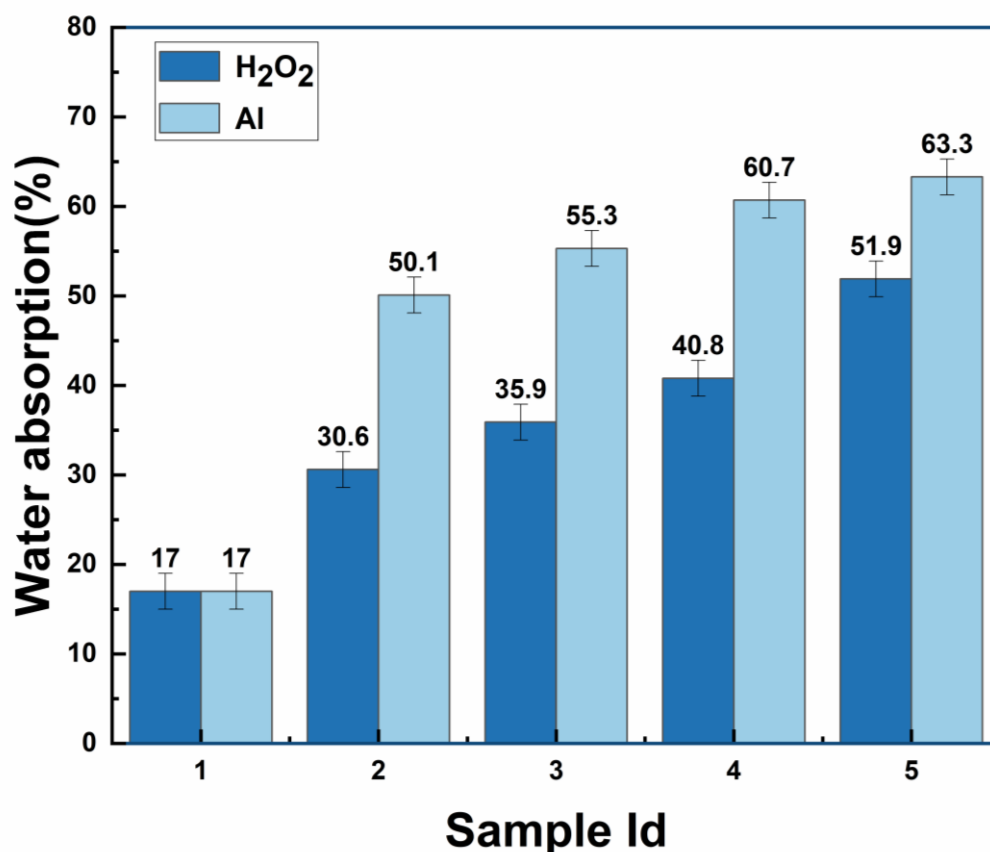


Figure 11. Water absorption (%) of HMNS-FA-phosphate-based porous geopolymers.

3.2. XRD Analysis

The phases of porous geopolymers were discussed after testing with XRD. As shown in Figure 12, the phases of porous geopolymers are mainly composed of forsterite, aluminum silicon phosphate, newberyite, forsterite ferron, AlPO_4 , quartz, and monetite. Among them, forsterite ferron, quartz, and mullite are the crystalline phases in HMNS and FA that are not involved in the reaction.

It can be seen from the graph that there is no difference in the phase composition of all specimens. This indicates that the blowing agent does not affect the end product of the ground polymerization reaction. The phases not involved in the reaction result in peaks that are more pronounced in the specimens with an added blowing agent. This indicates that the raw material is not fully involved in the reaction process in these specimens. From this, we can conclude that the geopolymerization reaction of porous geopolymers is reduced to varying degrees [45].

The XRD data indicate that the main products of the phosphate-based porous geopolymers are magnesite phosphate, aluminum silicon phosphate, and aluminum phosphate. The newberyite and aluminum silicon phosphate crystals as the skeleton and the colloid as the bonding agent allow the density of the geopolymer to increase, bringing about an improvement in the strength of the geopolymers [46]. These diffraction peaks become progressively stronger with time, indicating that the geopolymerization reaction continues, which makes the content of these crystals continue to grow. This fact coincides with the increasing strength of the porous geopolymer. The gel phase and crystals produced by the geopolymerization reaction increase the strength. The reaction products (AlPO_4) and forsterite in HMNS are both high-temperature-resistant phases [47]. This will facilitate the improvement of the high-temperature resistance of phosphate-based porous geopolymers.

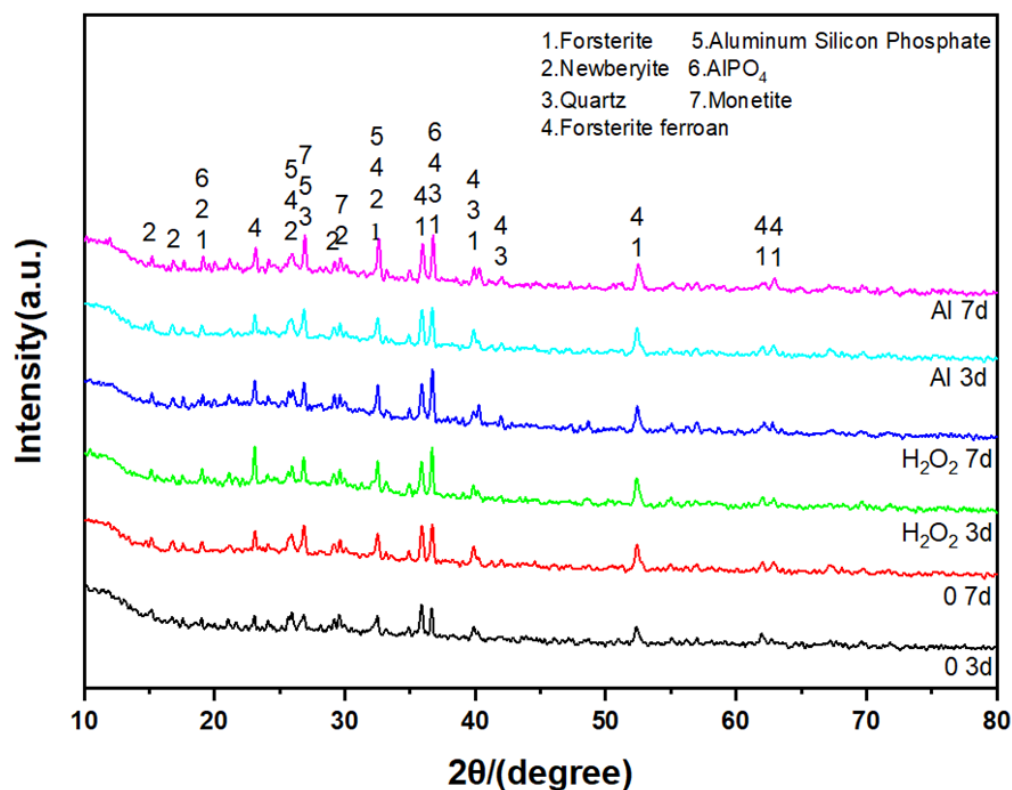


Figure 12. XRD patterns of the specimens prepared without a blowing agent and those prepared with different blowing agents.

3.3. FTIR Analysis

FTIR analysis was performed on specimens prepared in different ratios, as shown in Figure 13, to further investigate the microstructural composition of HMNS-FA-phosphate-based porous geopolymers. This reveals the presence of bound water inside the porous geopolymers prepared with phosphoric acid, which can be observed from the vibrational peaks that appear around 1645 cm^{-1} and 3450 cm^{-1} in Figure 13 [48]. These two vibrational peaks are the absorption bands of the -OH stretching and bending vibrations, respectively. The asymmetric stretching vibrations of Si(Al)-O-Si and Al-O-P-O lead to the absorption band at 1069 cm^{-1} [43]. The absorption peak at 793 cm^{-1} corresponds to the bending vibration of Al-O-P [49]; the absorption peak at 460 cm^{-1} should be the planar bending vibration of the Si-O or Al-O bonds [50]. The absorption bands at 510 cm^{-1} and 550 cm^{-1} are due to the stretching vibration of Mg-O [51]. The long chains of $[-\text{P}-\text{O}-\text{Al}-]_n$ and $[-\text{Si}-\text{O}-\text{Al}-\text{O}-\text{P}-]_n$ form the main polymeric structure of the phosphate-based porous geopolymers [36,43], which also corresponds to the formation of the phases detected in the XRD pattern (aluminum silicon phosphate and AlPO_4). The addition of the foaming agent did not change the geopolymerization reaction products of the phosphate-based geopolymer. This is because the position of the peaks did not change from one specimen to another. This conclusion can be corroborated with the previous data.

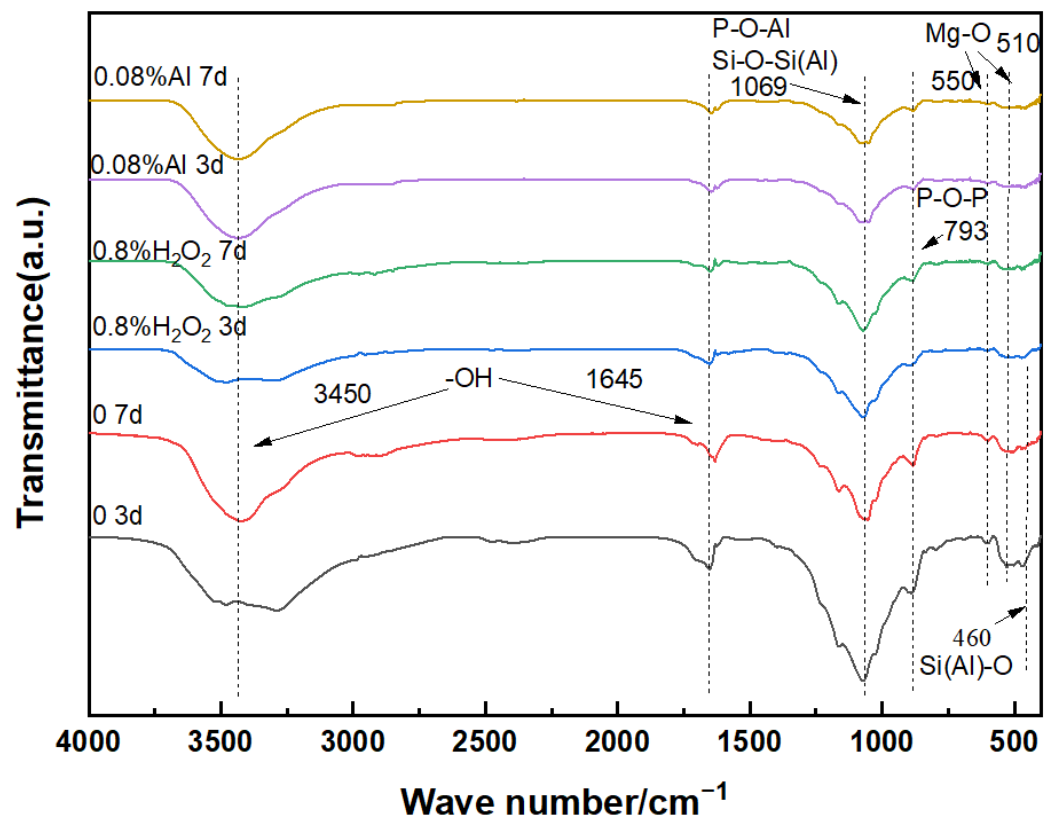


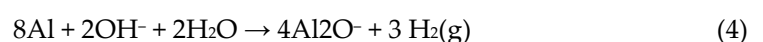
Figure 13. FTIR spectra of specimens prepared without a foaming agent and specimens prepared with different foaming agents.

3.4. Discussion

Consistent with the findings of Gu et al. [33], the factors influencing the density of a porous geopolymer also affect the material's strength. Specifically, for porous geopolymers, increasing the amount of almost all types of foaming agents leads to a decrease in both strength and density. The amount of foaming agent is also an important factor affecting thermal conductivity [52] and water absorption [53,54], as expected due to changes in porosity in the sample.

Based on the test analysis results of this study and a comparison with previous research conducted by others [46,55], we have summarized the geopolymerization mechanism of porous geopolymers. As shown in Figure 14, it mainly consists of the gas generation reaction and the geopolymerization reaction. Both occur simultaneously and interact with each other. This is the reason why the properties of porous geopolymers have changed.

The gas generation reaction: The two foaming agents react directly with the water in the slurry, producing $O_2(g)$ and $H_2(g)$ [36]. The gas generation process does not affect the products of the ground polymerization reaction. This is consistent with the results of XRD and FTIR analyses. The reaction equation is as follows:



As the geopolymerization reaction proceeds, the gas bubbles generated by the above reaction are trapped inside the specimen during the curing process. This creates voids or pores in the phosphate-base geopolymer that enhance its performance.

The geopolymerization reaction: After the mixed slurry is agitated sufficiently, phosphoric acid ionizes in the slurry to provide H^+ for the depolymerization reaction. The reaction equation is as follows:



The chemical bonds in the feedstock break in the presence of the H^+ in the above reaction. This step is the depolymerization process, which provides many ions and ionophores for the polycondensation process. These ionophores are interconnected to generate long chains of $[-\text{P}-\text{O}-\text{Al}-]_n$ and $[-\text{P}-\text{O}-\text{Al}-\text{O}-\text{Si}-]_n$. The long-chain units form the network structure of the porous geopolymer. As the polycondensation reaction proceeds, the AlPO_4 gel phase and the aluminum-silica phosphate gel phase are generated.

Due to the low activity of HMNS, it is difficult to start the reaction with phosphoric acid at an indoor temperature. The quartz and forsterite ferron in the feedstock did not fully participate in the chemical reaction or dissolve into the slurry. The gel phase wraps the other phases together to form the dense structure of the porous geopolymer. As the geopolymerization reaction continues, more of the gel phase is generated. The increase in the late strength of the porous geopolymer is attributed to the increase in the gel phase. It is important to note that the condensation process occurs when the depolymerization process takes place because the two are in dynamic equilibrium. The foaming agent simply provides a porous structure during the reaction. Al powder provides a few Al^{3+} when it is used as a foaming agent. However, its content is small and negligible.

HMNS did not have a heavily involved reaction, which is a good thing in a way. Forsterite ferron is a high-temperature resistant phase in theory. The geopolymerization reaction generates an aluminum phosphate gelling phase encapsulating forsterite ferron to enhance the high-temperature resistance of porous geopolymers. At the same time, the porous structure generated by the foaming process results in better insulation properties. This allows porous geopolymers to have better insulation potential in high-temperature environments.

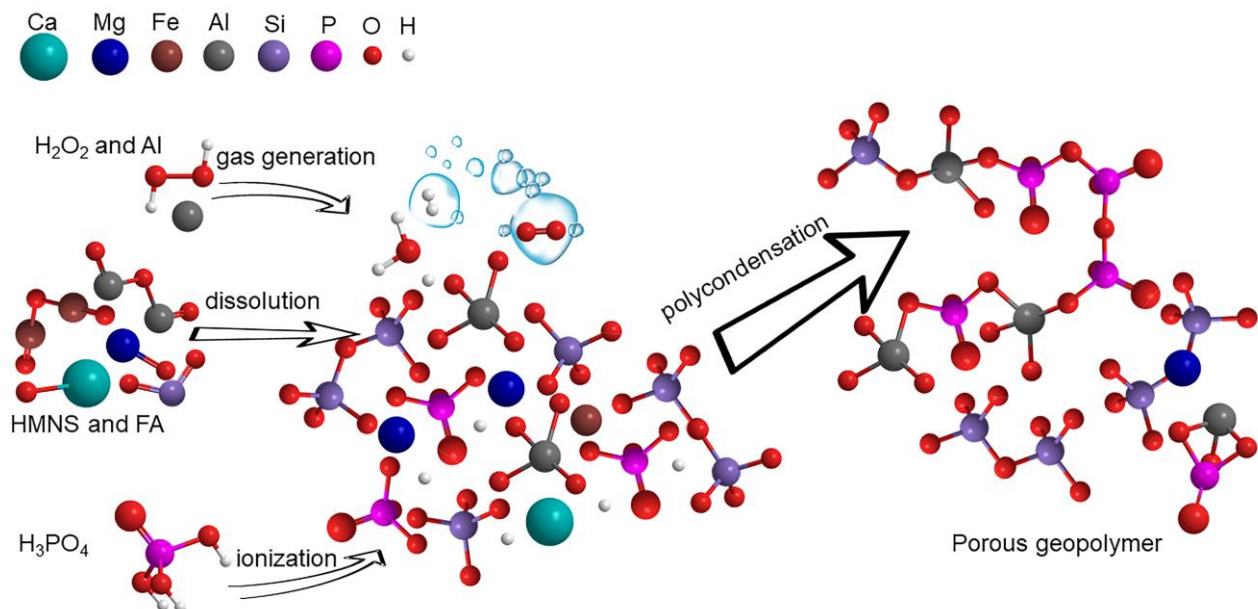


Figure 14. Geopolymerization reaction process of porous geopolymers.

4. Conclusions

The main reaction mechanisms involved in the formation of the HMNS-FA-phosphate-based porous geopolymers were physical encapsulation and chemical gelation. The foaming agent provided the system with a porous structure, which did not affect the

reaction products but hindered the degree of geopolymerization reaction. The porous structure, the generated aluminum phosphate, and the unreacted magnesium olivine all contributed to the excellent low thermal conductivity and refractory properties of the porous geopolymers. Moreover, the outstanding water absorption and compressive strength make the porous geopolymers have a broader application prospect, for example as an important component in the construction of sponge cities.

Author Contributions: Conceptualization, X.Y., Z.S., Y.W., Y.L., D.Z., D.X. and M.W.; Data curation, X.Y., Z.S., Y.W., Y.L., D.J. and D.Z.; Funding acquisition, D.X. and M.W.; Investigation, D.X.; Methodology, D.J. and M.W.; Software, X.Y., Z.S., Y.W., Y.L., D.Z., D.X. and M.W.; Validation, X.Y., Z.S., Y.W., Y.L. and D.J.; Writing—original draft, X.Y. and Z.S.; Writing—review & editing, X.Y. and M.W. All authors have read and agreed to the published version of the manuscript.

Funding: The authors acknowledge the financial support of the National Natural Science Foundation of China (51974168, 51662033), and State Key Laboratory of Silicate Materials for Architectures (Wuhan University of Technology) open fund grant (SYSJJ2020-08) is also appreciated.

Data Availability Statement: The datasets generated during and/or analyzed during the current study are available from the corresponding author on reasonable request.

Conflicts of Interest: The authors declare that they have no known competing financial interests or personal relationships that could have appeared to influence the work reported in this paper.

References

- Davidovits, J. Geopolymers and Geopolymeric Materials. *J. Therm. Anal.* **1989**, *35*, 429–441. <https://doi.org/10.1007/bf01904446>.
- Li, C.; Gong, X.; Cui, S.; Wang, Z.; Zheng, Y.; Chi, B. CO₂ Emissions due to Cement Manufacture. *Mater. Sci. Forum* **2011**, *685*, 181–187. <https://doi.org/10.4028/www.scientific.net/MSF.685.181>.
- Abbas, I.S.; Abed, M.H.; Canakci, H. Development and Characterization of Eco- And User-Friendly Grout Production via Mechanochemical Activation of Geopolymer. *J. Build. Eng.* **2022**, *63*, 105336. <https://doi.org/10.1016/j.jobe.2022.105336>.
- Freire, A.L.; José, H.J.; Moreira, R.D.F.P.M. Potential Applications For Geopolymers in Carbon Capture and Storage. *Int. J. Greenh. Gas Control* **2022**, *118*, 103687. <https://doi.org/10.1016/j.ijggc.2022.103687>.
- Li, J.; Liu, Y.; Ke, X.; Jiao, X.; Li, R.; Shi, C. Geopolymer Synthesized from Electrolytic Manganese Residue and Lead-Zinc Smelting Slag: Compressive Strength and Heavy Metal Immobilization. *Cem. Concr. Compos.* **2022**, *134*, 104806. <https://doi.org/10.1016/j.cemconcomp.2022.104806>.
- Raza, M.H.; Zhong, R.Y. A Sustainable Roadmap for Additive Manufacturing Using Geopolymers in Construction Industry. *Resour. Conserv. Recycl.* **2022**, *186*, 106592. <https://doi.org/10.1016/j.resconrec.2022.106592>.
- Abdulkareem, O.A.; Mustafa Al Bakri, A.M.; Kamarudin, H.; Khairul Nizar, I.; Saif, A.A. Effects of Elevated Temperatures on the Thermal Behavior and Mechanical Performance of Fly Ash Geopolymer Paste, Mortar And Lightweight Concrete. *Constr. Build. Mater.* **2014**, *50*, 377–387. <https://doi.org/10.1016/j.conbuildmat.2013.09.047>.
- Heah, C.Y.; Kamarudin, H.; Mustafa Al Bakri, A.M.; Bnhussain, M.; Luqman, M.; Khairul Nizar, I.; Ruzaidi, C.M.; Liew, Y.M. Study on Solids-To-Liquid and Alkaline Activator Ratios on Kaolin-Based Geopolymers. *Constr. Build. Mater.* **2012**, *35*, 912–922. <https://doi.org/10.1016/j.conbuildmat.2012.04.102>.
- Tzanakos, K.; Mimilidou, A.; Anastasiadou, K.; Stratakis, A.; Gidaracos, E. Solidification/Stabilization of Ash from Medical Waste Incineration into Geopolymers. *Waste Manag.* **2014**, *34*, 1823–1828. <https://doi.org/10.1016/j.wasman.2014.03.021>.
- Ul Haq, E.; Kunjalukkal Padmanabhan, S.; Licciulli, A. Synthesis and Characteristics of Fly Ash and Bottom Ash Based Geopolymers—a Comparative Study. *Ceram. Int.* **2014**, *40*, 2965–2971. <https://doi.org/10.1016/j.ceramint.2013.10.012>.
- Vickers, L.; Rickard, W.D.A.; Van Riessen, A. Strategies to Control the High Temperature Shrinkage of Fly Ash Based Geopolymers. *Thermochim. Acta* **2014**, *580*, 20–27. <https://doi.org/10.1016/j.tca.2014.01.020>.
- Ascensão, G.; Seabra, M.P.; Aguiar, J.B.; Labrincha, J.A. Red Mud-Based Geopolymers with Tailored Alkali Diffusion Properties and pH Buffering Ability. *J. Clean. Prod.* **2017**, *148*, 23–30. <https://doi.org/10.1016/j.jclepro.2017.01.150>.
- Ngouloure, Z.N.M.; Nait-Ali, B.; Zekeng, S.; Kamseu, E.; Melo, U.C.; Smith, D.; Leonelli, C. Recycled Natural Wastes in Metakaolin Based Porous Geopolymers for Insulating Applications. *J. Build. Eng.* **2015**, *3*, 58–69. <https://doi.org/10.1016/j.jobe.2015.06.006>.
- Novais, R.M.; Ascensão, G.; Seabra, M.P.; Labrincha, J.A. Waste Glass from End-Of-Life Fluorescent Lamps as Raw Material in Geopolymers. *Waste Manag.* **2016**, *52*, 245–255. <https://doi.org/10.1016/j.wasman.2016.04.003>.
- Novais, R.M.; Buruberri, L.H.; Ascensão, G.; Seabra, M.P.; Labrincha, J.A. Porous Biomass Fly Ash-Based Geopolymers with Tailored Thermal Conductivity. *J. Clean. Prod.* **2016**, *119*, 99–107. <https://doi.org/10.1016/j.jclepro.2016.01.083>.
- Novais, R.M.; Seabra, M.P.; Labrincha, J.A. Porous Geopolymer Spheres as Novel pH Buffering Materials. *J. Clean. Prod.* **2017**, *143*, 1114–1122. <https://doi.org/10.1016/j.jclepro.2016.12.008>.

17. Alzeer, M.I.M.; Mackenzie, K.J.D.; Keyzers, R.A. Porous Aluminosilicate Inorganic Polymers (Geopolymers): A New Class of Environmentally Benign Heterogeneous Solid Acid Catalysts. *Appl. Catal. A Gen.* **2016**, *524*, 173–181. <https://doi.org/10.1016/j.apcata.2016.06.024>.
18. Duan, P.; Yan, C.; Zhou, W.; Ren, D. Development of Fly Ash and Iron Ore Tailing Based Porous Geopolymer for Removal of CU(II) From Wastewater. *Ceram. Int.* **2016**, *42*, 13507–13518. <https://doi.org/10.1016/j.ceramint.2016.05.143>.
19. Feng, J.-J.; Zhang, R.-F.; Gong, L.-L.; Li, Y.; Cao, W.; Cheng, X.-D. Development of Porous Fly Ash-Based Geopolymer with Low Thermal Conductivity. *Mater. Des.* **2015**, *65*, 529–533. <https://doi.org/10.1016/j.matdes.2014.09.024>.
20. Minelli, M.; Medri, V.; Papa, E.; Miccio, F.; Landi, E.; Doghieri, F. Geopolymers as Solid Adsorbent for CO₂ Capture. *Chem. Eng. Sci.* **2016**, *148*, 267–274. <https://doi.org/10.1016/j.ces.2016.04.013>.
21. Novais, R.M.; Buruberri, L.H.; Seabra, M.P.; Bajare, D.; Labrincha, J.A. Novel Porous Fly Ash-Containing Geopolymers for pH Buffering Applications. *J. Clean. Prod.* **2016**, *124*, 395–404. <https://doi.org/10.1016/j.jclepro.2016.02.114>.
22. Novais, R.M.; Buruberri, L.H.; Seabra, M.P.; Labrincha, J.A. Novel Porous Fly-Ash Containing Geopolymer Monoliths for Lead Adsorption from Wastewaters. *J. Hazard. Mater.* **2016**, *318*, 631–640. <https://doi.org/10.1016/j.jhazmat.2016.07.059>.
23. Rouyer, J.; Benavent, V.; Frizon, F.; Poulesquen, A. Influence of Geopolymer Formulation Parameters on the Elastic and Porous Properties over a One-Year Monitoring. *Mater. Lett.* **2017**, *207*, 121–124. <https://doi.org/10.1016/j.matlet.2017.06.125>.
24. Li, X.; Li, J.; Bai, C.; Zheng, T.; Yang, K.; Zhang, X.; Qiao, Y.; Colombo, P. Preparation of Porous Slag-Based Geopolymer Spheres by Direct Template Route for pH Buffering Applications. *Mater. Lett.* **2022**, *328*, 133100. <https://doi.org/10.1016/j.matlet.2022.133100>.
25. Ma, S.; Liu, X.; Fu, S.; Zhao, S.; He, P.; Duan, X.; Yang, Z.; Jia, D.; Colombo, P.; Zhou, Y. Direct Ink Writing of Porous SiC Ceramics with Geopolymer as Binder. *J. Eur. Ceram. Soc.* **2022**, *42*, 6815–6826. <https://doi.org/10.1016/j.jeurceramsoc.2022.08.004>.
26. Wang, X.; Li, X.; Bai, C.; Qiao, Y.; Li, H.; Zhang, L.; Zhang, X.; Zheng, T.; Colombo, P. Facile Synthesis of Porous Geopolymers via the Addition of a Water-Soluble Pore Forming Agent. *Ceram. Int.* **2022**, *48*, 2853–2864. <https://doi.org/10.1016/j.ceramint.2021.10.075>.
27. Cui, Y.; Wang, D.; Zhao, J.; Li, D.; Serina, N.; Yafeng, R. Effect of Calcium Stearate Based Foam Stabilizer on Pore Characteristics and Thermal Conductivity of Geopolymer Foam Material. *J. Build. Eng.* **2018**, *20*, 21–29. <https://doi.org/10.1016/j.jobe.2018.06.002>.
28. Shao, N.; Zhang, Y.; Liu, Z.; Wang, D.; Zhang, Z. Fabrication of Hollow Microspheres Filled Fly Ash Based Foam Geopolymers with Ultra-Low Thermal Conductivity and Relative High Strength. *Constr. Build. Mater.* **2018**, *185*, 567–573. <https://doi.org/10.1016/j.conbuildmat.2018.07.077>.
29. Wu, J.; Zhang, Z.; Zhang, Y.; Li, D. Preparation and Characterization of Ultra-Lightweight Foamed Geopolymer (ufg) Based on Fly Ash-Metakaolin Blends. *Constr. Build. Mater.* **2018**, *168*, 771–779. <https://doi.org/10.1016/j.conbuildmat.2018.02.097>.
30. Hajimohammadi, A.; Ngo, T.; Priyan, M. Enhancing the Strength of Pre-made Foams for Foam Concrete Applications. *Cem. Concr. Compos.* **2018**, *87*, 164–171. <https://doi.org/10.1016/j.cemconcomp.2017.12.014>.
31. Degefu, D.M.; Liao, Z.; Berardi, U.; Labbé, G. The Dependence of Thermophysical and Hygroscopic Properties of Macro-Porous Geopolymers on Si/Al. *J. Non-Cryst. Solids* **2022**, *582*, 121432. <https://doi.org/10.1016/j.jnoncrysol.2022.121432>.
32. Ettahiri, Y.; Bouna, L.; Hanna, J.V.; Benhachemi, A.; Pilsworth, H.L.; Bouddouch, A.; Bakiz, B. Pyrophyllite Clay-Derived Porous Geopolymers for Removal of Methylene Blue from Aqueous Solutions. *Mater. Chem. Phys.* **2023**, *296*, 127281. <https://doi.org/10.1016/j.matchemphys.2022.127281>.
33. Gu, G.; Xu, F.; Ruan, S.; Huang, X.; Zhu, J.; Peng, C. Influence of Precast Foam on the Pore Structure and Properties of Fly Ash-Based Geopolymer Foams. *Constr. Build. Mater.* **2020**, *256*, 119410. <https://doi.org/10.1016/j.conbuildmat.2020.119410>.
34. Guo, Z.; Wang, Y.; Li, S.; Pan, J.; Deqing, Z.; Congcong, Y.; Liaoting, P.; Hongyu, T.; Wang, D. Reductive Roasting Mechanism of Copper Slag and Nickel Laterite for Fe-Ni-Cu Alloy Production. *J. Mater. Res. Technol.* **2020**, *9*, 7602–7614. <https://doi.org/10.1016/j.jmrt.2020.04.0>.
35. Xi, B.; Li, R.; Zhao, X.; Dang, Q.; Zhang, D.; Tan, W. Constraints and Opportunities for the Recycling of Growing Ferronickel Slag in China. *Resour. Conserv. Recycl.* **2018**, *139*, 15–16. <https://doi.org/10.1016/j.resconrec.2018.08.002>.
36. Dhasindrakrishna, K.; Pasupathy, K.; Ramakrishnan, S.; Sanjayan, J. Progress, Current Thinking and Challenges in Geopolymer Foam Concrete Technology. *Cem. Concr. Compos.* **2021**, *116*, 103886. <https://doi.org/10.1016/j.cemconcomp.2020.103886>.
37. Gopalakrishna, B.; Dinakar, P. Mix Design Development of Fly Ash-Ggbs Based Recycled Aggregate Geopolymer Concrete. *J. Build. Eng.* **2022**, *63*, 105551. <https://doi.org/10.1016/j.jobe.2022.105551>.
38. Luna-Galiano, Y.; Leiva, C.; Arroyo, F.; Villegas, R.; Vilches, L.; Fernández-Pereira, C. Development of Fly Ash-Based Geopolymers Using Powder Sodium Silicate Activator. *Mater. Lett.* **2022**, *320*, 132346. <https://doi.org/10.1016/j.matlet.2022.132346>.
39. Somna, R.; Saowapun, T.; Somna, K.; Chindapasirt, P. Rice Husk Ash and Fly Ash Geopolymer Hollow Block Based on NaOH Activated. *Case Stud. Constr. Mater.* **2022**, *16*, e01092. <https://doi.org/10.1016/j.cscm.2022.e01092>.
40. Trincal, V.; Multon, S.; Benavent, V.; Lahalle, H.; Balsamo, B.; Caron, A.; Bucher, R.; Diaz Caselles, L.; Cyr, M. Shrinkage Mitigation of Metakaolin-Based Geopolymer Activated by Sodium Silicate Solution. *Cem. Concr. Res.* **2022**, *162*, 106993. <https://doi.org/10.1016/j.cemconres.2022.106993>.
41. Zhang, B.; Yu, T.; Deng, L.; Li, Y.; Guo, H.; Zhou, J.; Li, L.; Peng, Y. Ion-Adsorption Type Rare Earth Tailings for Preparation of Alkali-Based Geopolymer with Capacity for Heavy Metals Immobilization. *Cem. Concr. Compos.* **2022**, *134*, 104768. <https://doi.org/10.1016/j.cemconcomp.2022.104768>.

42. Verma, C.; Madan, S.; Hussain, A.; Dubey, S. Heavy Metal Contamination of Groundwater Due to Fly Ash Disposal of Coal-Fired Thermal Power Plant, Parichha, Jhansi, India. *Cogent Eng.* **2016**, *3*, 1179243. <https://doi.org/10.1080/23311916.2016.1179243>.
43. Derouiche, R.; Baklouti, S. Phosphoric Acid Based Geopolymerization: Effect of the Mechanochemical and the Thermal Activation of the Kaolin. *Ceram. Int.* **2021**, *47*, 13446–13456. <https://doi.org/10.1016/j.ceramint.2021.01.203>.
44. Qoku, E.; Scheibel, M.; Bier, T.; Gerz, A. Phase Development of Different Magnesium Phosphate Cements at Room Temperature and Elevated Temperatures. *Constr. Build. Mater.* **2021**, *272*, 121654. <https://doi.org/10.1016/j.conbuildmat.2020.121654>.
45. Ji, Z.; Li, M.; Su, L.; Pei, Y. Porosity, Mechanical Strength and Structure of Waste-Based Geopolymer Foams by Different Stabilizing Agents. *Constr. Build. Mater.* **2020**, *258*, 119555. <https://doi.org/10.1016/j.conbuildmat.2020.119555>.
46. Li, J.; Sun, Z.; Wang, L.; Yang, X.; Zhang, D.; Zhang, X.; Wang, M. Properties and Mechanism of High-Magnesium Nickel Slag-Fly Ash Based Geopolymer Activated by Phosphoric Acid. *Constr. Build. Mater.* **2022**, *345*, 128256. <https://doi.org/10.1016/j.conbuildmat.2022.128256>.
47. Zhang, Z.; Zhu, Y.; Yang, T.; Li, L.; Zhu, H.; Wang, H. Conversion of Local Industrial Wastes into Greener Cement through Geopolymer Technology: A Case Study of High-Magnesium Nickel Slag. *J. Clean. Prod.* **2017**, *141*, 463–471. <https://doi.org/10.1016/j.jclepro.2016.09.147>.
48. Pu, S.; Zhu, Z.; Wang, W.; Duan, W.; Wu, Z.; Li, N.; Jiang, P. Water Resistance of Fly Ash Phosphoric Acid-Based Geopolymer. *Dev. Built Environ.* **2022**, *12*, 100093. <https://doi.org/10.1016/j.dibe.2022.100093>.
49. Liu, Y.; Meng, Y.; Qiu, X.; Zhou, F.; Wang, H.; Zhou, S.; Yan, C. Novel Porous Phosphoric Acid-Based Geopolymer Foams for Adsorption of Pb(II), Cd(II) And Ni(II) Mixtures: Behavior and Mechanism. *Ceram. Int.* **2022**, *49*, 7030–7039. <https://doi.org/10.1016/j.ceramint.2022.10.164>.
50. Tchakouté, H.K.; Bewa, C.N.; Fotio, D.; Dieuhou, C.M.; Kamseu, E.; Rüscher, C.H. Influence of Alumina on the Compressive Strengths and Microstructural Properties of the Acid-Based Geopolymers from Calcined Indurated Laterite and Metakaolin. *Appl. Clay Sci.* **2021**, *209*, 106148. <https://doi.org/10.1016/j.clay.2021.106148>.
51. Leping, L.; Xuemin, C.; Shuheng, Q.; Junli, Y.; Lin, Z. Preparation of Phosphoric Acid-Based Porous Geopolymers. *Appl. Clay Sci.* **2010**, *50*, 600–603. <https://doi.org/10.1016/j.clay.2010.10.004>.
52. Karakaş, H.; İlkentapar, S.; Durak, U.; Örklemmez, E.; Özuzun, S.; Karahan, O.; Atiş, C.D. Properties of Fly Ash-Based Lightweight-Geopolymer Mortars Containing Perlite Aggregates: Mechanical, Microstructure, and Thermal Conductivity Coefficient. *Constr. Build. Mater.* **2023**, *362*, 129717. <https://doi.org/10.1016/j.conbuildmat.2022.129717>.
53. Kamseu, E.; Ngouloure, Z.N.M.; Tiogning-Djiogue, L.K.; Andreola, F.; Nait-Ali, B.; Rossignol, S.; Leonelli, C. Enhancing Hygroscopic Capacities of Metakaolin Based Porous Insulating Geopolymers: Comparative Effects of Calcium Silicate and Sodium Polyacrylate. *J. Build. Eng.* **2023**, *67*, 106020. <https://doi.org/10.1016/j.jobe.2023.106020>.
54. Yu, Y.; Perumal, P.; Corfe, I.J.; Paul, T.; Illikainen, M.; Luukkonen, T. Combined Granulation–Alkali Activation–Direct Foaming Process: A Novel Route to Porous Geopolymer Granules with Enhanced Adsorption Properties. *Mater. Des.* **2023**, *227*, 111781. <https://doi.org/10.1016/j.matdes.2023.111781>.
55. He, M.; Yang, Z.; Li, N.; Zhu, X.; Fu, B.; Ou, Z. Strength, Microstructure, CO₂ Emission and Economic Analyses of Low Concentration Phosphoric Acid-Activated Fly Ash Geopolymer. *Constr. Build. Mater.* **2023**, *374*, 130920. <https://doi.org/10.1016/j.conbuildmat.2023.130920>.

Disclaimer/Publisher’s Note: The statements, opinions and data contained in all publications are solely those of the individual author(s) and contributor(s) and not of MDPI and/or the editor(s). MDPI and/or the editor(s) disclaim responsibility for any injury to people or property resulting from any ideas, methods, instructions or products referred to in the content.